Nuclear Science and Techniques (2026) 37:42
https://doi.org/10.1007/s41365-025-01862-6

Biomass aerogel based on chitosan and bayberry tannin for uranium recovery from aqueous solution

Gui-Qiang He[1,2] · Jin-Fan Ou[1] · Yan-Xia Wei[1,2] · Ai-Xia Lu[1] · Dan Lin[3] · Jian Zhou[1,2]

Received: 27 May 2024 / Revised: 11 September 2024 / Accepted: 16 September 2024 / Published online: 9 January 2026

Abstract

Many adsorbents have been developed for uranium recovery to ensure global energy and environmental security. However, most reported adsorbents involve complex preparation process and rely heavily on petrochemical feedstocks, which undoubtedly increases carbon emissions from production in the nuclear industry. Here, a biomass aerogel (CS-BT) is prepared by the facile cross-linking of chitosan and bayberry tannins with glutaraldehyde. U(VI) can be adsorbed by hydroxyl groups on CS-BT aerogel via chelation, and the maximum adsorption capacity of the obtained aerogel to U(VI) is 140 mg · g^{-1} and the removal rate reaches up to 99% (at 298.15 K, pH = 5.0). The pseudo-second-order kinetics model and Freundlich model can better match the adsorption process of CS-BT aerogel, implying that its adsorption is a chemical adsorption process dominated by multilayer adsorption. The thermodynamic results show that the adsorption process of U(VI) by CS-BT aerogel is spontaneous and exothermic. Hence, our biomass aerogel can effectively extract uranium from water, contributing to the sustainable development of the nuclear industry.

Keywords Biomass aerogel · Chitosan · Bayberry tannin · Uranium recovery

1 Introduction

Limited resource availability, uncontrolled population growth, and global environmental degradation have aroused interest in accessing sustainable clean energy resources. The nuclear fuel based on uranium is a new clean energy source, whose fission releases much more energy than that released by burning coal, effectively avoiding the emission of the greenhouse gas carbon dioxide [1, 2]. However, uranium-containing wastes from the nuclear fuel cycle or nuclear accidents are both radioactive and chemically toxic [3]. Uranium has a half-life of millions of years, and it can be easily transferred to the water environment when there is a slight change in the environmental condition, causing chronic pollution [4]. At the same time, large uranium reserves are necessary for energy security and greenhouse gas mitigation. Therefore, developing efficient technologies for the removing and recovering uranium from nuclear industry wastewater or other solutions for ensuring environmental safety and building up nuclear energy reserves is essential.

Current research efforts are heavily focused on extracting U(VI) (the predominant aqueous species of uranium) from diverse uranium-laden solutions, including nuclear industry wastewater and seawater, mainly concentrating on adsorption [5, 6], ion exchange [7], membrane separation [8, 9], and solvent extraction [10]. Among them, adsorption is the most common and effective approach for uranium extraction and removal of other organic and inorganic contaminants,

This work was supported by Doctoral Scientific Fund Project of Southwest University of Science and Technology (20zx7130) and Seawater Uranium Extraction Innovation and Development Fund Project (China National Nuclear Corporation) (CNNC-CXLM-202215).

✉ Gui-Qiang He
guiqianghe@swust.edu.cn

✉ Jian Zhou
zhoujian@swust.edu.cn

[1] School of Life Science and Engineering, Southwest University of Science and Technology, Mianyang 621010, China

[2] Engineering Research Center of Biomass Materials, Ministry of Education, Southwest University of Science and Technology, Mianyang 621010, China

[3] West Sichuan International Technology Transfer Center, Chengdu 610000, China

owing to its cost-effectiveness and operational simplicity [11–15]. At present, various types of adsorbents have been successfully developed, including metal/covalent organic frameworks [6, 16], synthetic organic polymers [17], and carbon-based adsorbents [18]. However, most of these reported adsorbents are synthetic materials based on petrochemicals, which still increases global carbon emission during the production of nuclear industry.

In response to the current increasingly serious environmental problems, people are turning their attention from petrochemical products to biomass materials due to the latter's many unique advantages such as eco-friendliness, abundant sources, and a large number of reactive groups that can interact with the target adsorbate [19, 20]. Hence, biomass-based adsorbents are emerging [21–23]. For example, Wang et al. synthesized amidoximated cellulose fibers by grafting polyacrylonitrile (PAN) onto cellulose fibers and amidoxime modification to extraction uranium from seawater [24]. Ye and his workers designed a new uranium extraction material by grafting phosphoric acid and amidoxime groups onto skin collagen fibers for uranium extraction from seawater [25]. On the other hand, aerogel adsorption materials have attracted extensive attention of many experts and scholars in recent years because of their high porosity, high specific surface area, and exceptional adsorption performance in the application of uranium extraction from aqueous solutions [26]. For instance, Chen et al. developed unique carbon-encapsulated zero-valent iron nanoparticles using konjac glucomannan-derived carbon aerogel for reduction-assisted uranium extraction [27]. In addition, other biomass aerogels, such as feather keratin [28], chitosan [29], and microalgae aerogels [30], have been widely reported and used for recovering uranium. Although the biomass materials are used in these reported biomass-based adsorbents, their preparation process includes complex multi-step chemical reactions and the usage of large amounts of petrochemical feedstocks. To pursue as green and low carbon as possible for the uranium extraction process, developing biomass aerogels through a facile method and using as many biomass feedstocks as available is very significant.

Tannin, a naturally occurring polyphenol extracted from plants, ranks among the most abundant biomass feedstocks in nature. And the plant tannin includes abundant phenolic hydroxyls, which can form five-member rings to chelate multiple metal ions [31, 32]. Hence, the polyphenol-based adsorbent is a promising material for extracting uranium from various aqueous solutions. However, tannins cannot be directly applied for uranium extraction due to their high water solubility. Thus, they must be embedded within a solid matrix prior to use. The chitosan is also a biomass material with abundant active groups such as -OH and -NH_2 groups and has been used to prepare adsorbents for adsorbing metal ions from aqueous solutions [33–35]. Meanwhile, since the chitosan is water-soluble in acidic conditions, it usually also needs to be solidified similarly. Based on the above statement, we believe that the preparation of biomass aerogels with a 3D network structure by facile cross-linking tannins with chitosan is promising in uranium extraction from seawater, which is expected to meet the green demands of uranium recovery process as much as possible.

Herein, we fabricated a biomass aerogel by the facile cross-linking of chitosan and bayberry tannins with glutaraldehyde. This aerogel maximizes the use of animal- and plant-derived biomass feedstocks. The as-prepared CS-BT aerogel has a 3D porous network structure and numerous reactive groups that can interact with uranium, allowing it to be used for uranium adsorption from aqueous solutions. Adsorption experiments were conducted to evaluate its adsorption performances, while kinetic and thermodynamic studies were carried out to propose the appropriate adsorption models. Finally, the adsorption mechanism was summarized via multiple characterization methods. This work contributes to further reducing the use of chemical feedstocks in the uranium recovery process, thereby reducing carbon emissions and promoting environmentally sustainable development.

2 Experiment

2.1 Materials

Uranyl nitrate (99%, AR) was offered by Hubei Chushengwei Chemical Co., Ltd. Glutaraldehyde (50 wt% aqueous solution, AR) and acetic acid (99%, AR) were purchased from Chengdu Kelong Chemical Co., Ltd. Chitosan (CS, BR, 85%, deacetylation degree ≥ 90%, Mw:~100000) was purchased from Shanghai Macklin Biochemical Technology Co., Ltd. Bayberry tannin (BT, industrial grade, 66%) was purchased from Guangxi Baise Forest Chemical Factory. Arsenazo III was obtained from Shanghai Linen Technology Development Co., Ltd. Uranium standard solution was offered by Beijing Institute of Chemical Metallurgy for Nuclear Industry.

2.2 Preparation of CS-BT aerogel

Firstly, the deionized water (600 mL) was added to a beaker (1 L) with BT (3 g) and stirred (300 r/min at 25 °C) for 2 h to completely dissolve BT. Then, CS (3 g) and acetic acid (6 mL) were added to the beaker and continuously stirred for 2 h. After completely dissolving CS, the glutaraldehyde (1.5 mL) was added to the beaker and put into the thermostatic shaking box (150 r/min at 45 °C) for 24 h. After that, the prepared sol was transferred into a plastic Petri dish. Deionized water was added and decanted three times to thoroughly

wash away any unreacted reagents.. Finally, after freezing in a refrigerator at −80 °C for 12 h, the CS-BT composite aerogel was obtained by freeze-drying for 72 h.

2.3 Characterizations of CS-BT aerogel

X-ray photoelectron spectroscopy (XPS) analysis was performed on an X-ray photoelectron spectrometer (Thermo Fisher K-Alpha, USA) with a monochromatic Al X-ray radiation source. Fourier transform infrared (FTIR) spectra were tested from 4000 to 500 cm^{-1} on an infrared spectrometer (Thermo Fisher Nicolet iS50, USA) with a potassium bromide tableting method. The microscopic morphology of samples was observed by field emission scanning electron microscopy (FE-SEM, Carl Zeiss Ultra55, Germany) at 200 kV. Nitrogen adsorption and desorption isotherms were tested at the liquid nitrogen temperature with an automatic surface area and porosity analyzer (Micromeritics ASAP 2460, USA).

2.4 Adsorption of uranium by CS-BT aerogel

2.4.1 Test method of uranium ion and BT

Uranium ion standard solution (1000 $mg \cdot L^{-1}$), dilute hydrochloric acid solution (0.1 $mol \cdot L^{-1}$), and arsenazo III solution (1 $g \cdot L^{-1}$) were used to accurately prepare the uranium test solution with different concentrations of 0, 1, 2, 3, 4, and 5 $mg \cdot L^{-1}$ under different pH. After that, these solutions were measured on an enzyme marker (Molecular SpectraMax 190, USA) to establish a standard curve of uranium content based on absorbance.

On the other hand, BT solutions with different concentrations (0.02, 0.04, 0.06, 0.08, 0.1, 0.12, and 0.14 $g \cdot L^{-1}$) were also prepared. After that, these solutions were measured with an ultraviolet spectrophotometer (Hitachi UV-3900, Japan) within the wavelength range of 200 to 400 nm to establish a standard curve of BT content between absorbance.

2.4.2 Effects of solution pH and adsorbent mass on adsorption

Firstly, 20 $mg \cdot L^{-1}$ uranyl nitrate solutions with different pH (3.0, 4.0, 5.0, 6.0, 7.0, and 8.0) were prepared. Then, the as-prepared U(VI) solution (50 mL) and aerogel with different masses (0.005, 0.01, 0.02, 0.03, 0.04, 0.06, and 0.08 g) were placed in a conical flask and shaken in a thermostatic shaking box (150 r/min at 45 °C) for 24 h. After that, the solution was filtered, and the U(VI) concentration was tested and calculated. For each adsorption experiment, at least three repetitions were performed to minimize operator error. The adsorption capacity (A_c, $mg \cdot g^{-1}$) and removal rate (R_r, %) of U(VI) were calculated by the following equations:

$$A_c = (C_0 - C_e) \times V/m, \tag{1}$$

$$R_r = (C_0 - C_e)/C_0 \times 100\%, \tag{2}$$

where C_0 ($mg \cdot L^{-1}$) and C_e ($mg \cdot L^{-1}$) are the concentration of U(VI) before and after adsorption, respectively; V is the volume of the solution (L); m (g) represents the mass of adsorbent.

2.4.3 Cyclic adsorption

Firstly, 20 mg of CS-BT aerogel, which had adsorbed uranium, was placed in a 150-mL conical flask. Then 50 mL of 0.1 $mol \cdot L^{-1}$ HCl solution was added to the conical flask for desorption at 25 °C for 24 h. After desorption was completed, the CS-BT aerogel was washed trice with 100 mL of distilled water and dried at 45 °C. This cycle was repeated five times, and the adsorption capacity was calculated.

2.4.4 Adsorption kinetics

The kinetics experimental values were obtained from 20 $mg \cdot L^{-1}$ uranyl nitrate solution and linearly fitted by pseudo-first-order model and pseudo-second-order kinetics models, and they can be expressed by the following two equations, respectively:

$$\ln(q_e - q_t) = \ln q_e - K_1 t, \tag{3}$$

$$t/q_t = 1/K_2 q_e^2 + t/q_e, \tag{4}$$

where K_1 and K_2 ($g \cdot mg^{-1} \cdot min^{-1}$) represent rate constants for the pseudo-first-order and pseudo-second-order kinetics models, respectively, t is the time of adsorption of U(VI), and q_t and q_e ($mg \cdot g^{-1}$) are the adsorption capacity at specific time and equilibrium, respectively.

The isothermal experimental values were linearly fitted by Langmuir and Freundlich isotherm models, which can be expressed by the following two equations, respectively:

$$q_e = K_L q_m C_e/(1 + K_L C_e), \tag{5}$$

$$q_e = K_F C_e^{1/n}, \tag{6}$$

where C_e ($mg \cdot L^{-1}$) is the residual concentration of metal ions in solution at equilibrium, q_m is maximum adsorption capacity of the gel, K_L ($L \cdot mg^{-1}$) is the Langmuir isotherm adsorption constant, K_F ($(mg \cdot g^{-1})(L \cdot mg^{-1})^{1/n}$) is the Freundlich isotherm adsorption constant, and n is the empirical constant.

2.4.5 Adsorption thermodynamics

The isothermal experimental values were obtained from uranyl nitrate solutions with different concentrations (20, 80 140, 240, and 300 mg · L^{-1}) over a wide temperature range and linearly fitted by the following three equations, respectively:

$$\ln q_e = -\Delta H^0/R \times 1/T + \Delta S^0/R, \quad (7)$$

$$\Delta G^0 = -RT\ln K_0, \quad (8)$$

$$K_0 = q_m \times K_L, \quad (9)$$

where R is the ideal gas constant (8.314×10^{-3} kJ · mol^{-1} · K^{-1}), T is the Kelvin temperature (K), K_0 (mL/g) is the adsorption equilibrium constant. ΔG^0, ΔH^0, and ΔS^0 are the values of Gibbs energy, enthalpy, and entropy variations, respectively.

2.4.6 Effects of coexisting ions on adsorption

20 mg · L^{-1} uranyl nitrate solution containing coexisting ions (2 mg · L^{-1} Cd^{2+}, Ni^{2+}, VO_3^-, Fe^{3+}, and Pb^{2+}) was prepared. The effect of a single coexisting ion on the adsorption process was investigated within 2 h by testing the adsorption rate.

3 Results and Discussion

3.1 Preparation and characterizations of CS-BT aerogel

The schematic diagram of the preparation of CS-BT aerogel is shown in Fig. 1a. First CS and BT completely dissolved to form a complex solution under stirring. Then, the glutaraldehyde, acting as a chemical cross-linking agent, was added to the complex solution, facilitating the grafting or cross-linking between BT and CS. In this process, the glutaraldehyde

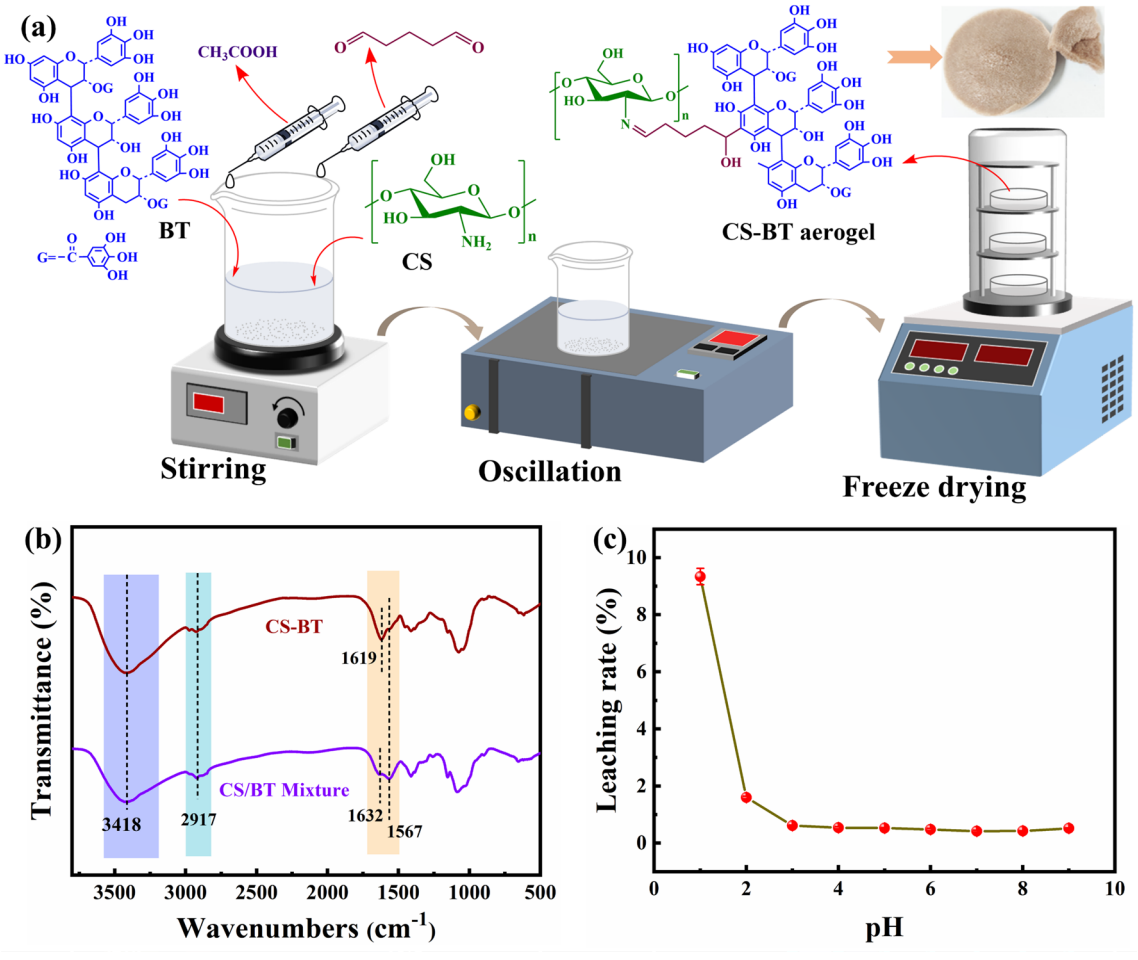

Fig. 1 (Color online) **a** Preparation schematic diagram of CS-BT aerogel. **b** FTIR spectra of CS-BT and CS/BT mixture. **c** Leaching rate of bayberry tannin at different pH

could undergo a Schiff base reaction with -NH_2 on CS and a Mannich reaction with C6 and C8 reactive hydrogens on BT to form covalent bonds, which ensures successful functionalization of CS by BT [32].

FTIR spectra of CS-BT aerogel and CS/BT mixture are shown in Fig. 1b. The band at 3418 cm^{-1} could be assigned to the stretching vibration of -NH_2 and -OH, and the band at 2917 cm^{-1} was related to the stretching vibration of C-H. Moreover, the benzene skeleton vibration BT could also be observed at 1632 cm^{-1} and 1567 cm^{-1}. However, compared with the CS/BT mixture, there was a significant difference in the peak intensity of CS-BT at 1632 cm^{-1}, and it became stronger and shifted to 1619 cm^{-1}. This can be attributed to the formation of C=N by the Schiff base reaction between -NH_2 and aldehyde groups [36–38]. On the other hand, C=N bonds are usually not stable under a strong acidic environment. Hence, the BT leaching experiment of BT was carried out at different pH levels. As shown in Fig. 1c, the leaching rate of BT was less than 1% at pH > 3.0. This indicates that BT has been successfully grafted to CS.

The microscopic morphology of CS-BT aerogel was characterized by SEM. As shown in Fig. 2a and b, it could be clearly seen that the inner part of CS-BT aerogel is loose and porous, with a three-dimensional network structure, and the pore size is between ten and twenty microns. This indicates that CS-BT aerogel has the advantages of being light weight, having higher porosity, and having a large specific surface area, which increases the contact area with metal ions and the adsorption sites during adsorption. To further quantify the porous feature, the nitrogen adsorption and desorption isotherms for CS-BT aerogel were investigated. As presented in Fig. 2c, the nitrogen adsorption and desorption isotherms belonged to typical type IV. It was observed that the nitrogen adsorption volume increased gradually in the low-pressure region but sharply in the high-pressure region, suggesting the presence of both micro- and mesopores in the synthesized CS-BT aerogel [17]. This resultant is consistent with SEM images. Moreover, the specific surface area of CS-BT aerogel calculated by the Brunauer–Emmett–Teller (BET) method was 26.06 $cm^2 \cdot g^{-1}$, and its average pore size was 10.33 nm. The presence of many a large number of pores and a high specific surface area in the CS-BT aerogel provides favorable circumstances for the diffusion of metal ions into its interior.

3.2 Adsorption performances

3.2.1 Effects of solution pH on adsorption

pH is closely related to the chemical activity of metal ions and the ionization of adsorbent functional groups [39]. Hence, the effect of solution pH on the uranium adsorption was investigated. As shown in Fig. 3a, the adsorption rate of 0.06 g CS-BT aerogel on U(VI) increased gradually when the solution pH increased from 3.0 to 5.0. The adsorption efficiency was smaller when the pH was lower, which was because due to the fact that the surface amino groups of CS-BT aerogel were positively charged after protonation, increasing the electrostatic repulsion between U(VI) and amino groups, thus reducing the adsorption effect of CS-BT aerogel. When pH value increased from 5.0 to 8.0, the adsorption rate almost reached equilibrium, with maximum efficiency of approximately 99%, which may be attributed to the fact that the uranyl ion in the solution is positively charged $[(UO_2)_x(OH)_y]^{z+}$ [40], and the degree of protonation for amino groups decreases, thus weakening the electrostatic repulsion to promote the adsorption capacity of uranium. And the CS-BT aerogel was gradually deprotonated, and more carboxyl groups were dissociated into the carboxylate ions with negative charge, which provided more active sites for the adsorption of U(VI). The adsorption rate is higher at pH 5.0, so the subsequent experiments were carried out at pH 5.0.

3.2.2 Effect of CS-BT aerogel mass on adsorption

The amount of adsorbent determines the number of adsorption active sites during operation. As shown in Fig. 3b, the adsorption rate increased significantly with increasing mass of CS-BT aerogel, with 98% at 0.02 g CS-BT aerogel. The

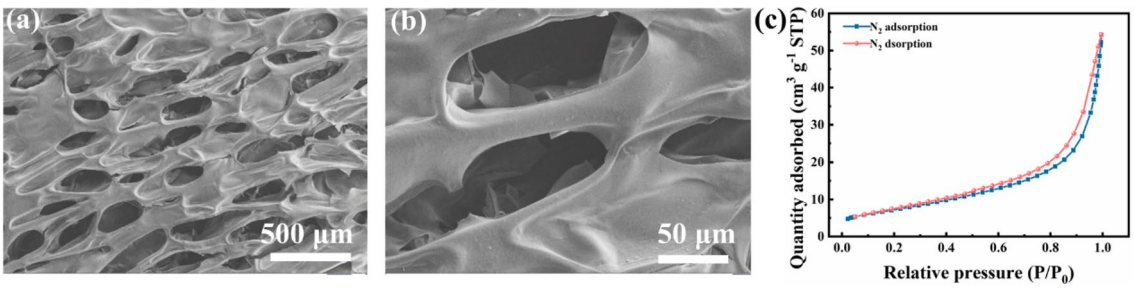

Fig. 2 (Color online) **a**, **b** SEM images of CS-BT aerogel. **c** Nitrogen adsorption and desorption curves of CS-BT aerogel

adsorption rate of CS-BT aerogel was higher than that of previously reported aerogels, such as feather keratin (92%) [28], chitosan/amidoxime polyacrylonitrile (91%) [29], and microalgae (85%) aerogels [30]. The adsorption rate no longer increased when the adsorbent mass continuously increased. However, the adsorption capacity kept decreasing with the increase in the adsorbent amount. This is because at the same concentration of U(VI), the continuous increase in the mass of adsorbent caused a decrease in the adsorption capacity per unit mass of aerogel. Based on adsorption efficiency and cost considerations, CS-BT aerogel was quantified as 0.02 g in the subsequent experiments. Moreover, the cyclic adsorption was also performed. As shown in Fig. 3c, the adsorption capacity only slightly reduced, from 44.6 to 37.4 mg · g^{-1}, showing a potential reusability.

3.3 Adsorption kinetics

Adsorption kinetics is an effective method for assessing the efficiency of an adsorbent. The adsorption kinetics curves of CS-BT aerogel are shown in Fig. 4a. With the increase of adsorption time, the adsorption rate and capacity also significantly improved. After 180 min, the adsorption rate was exceeded 80%. Subsequently, the adsorption almost reached equilibrium at about 600 min, with the adsorption rate of 95.09% and adsorption capacity of 45.4 mg · g^{-1}, respectively. Initially, U(VI) rapidly bound bind to the active adsorption sites on the surface of CS-BT aerogel, showing a higher adsorption rate. Then, U(VI) spread and migrated from the outside to the inside of CS-BT aerogel, and the adsorption rate continued to grow due to the high ion concentration difference between the inside and outside of CS-BT aerogel. As more active sites on CS-BT aerogel were gradually bound by U(VI), the adsorption rate no longer changed significantly, reaching adsorption equilibrium.

To deepen the insight into the adsorption mechanism of CS-BT aerogel, the kinetics data were further fitted by the pseudo-first-order and pseudo-second-order kinetics models. The fitting results are shown in Fig. 4b and c and Table 1. The correlation coefficients (R^2) of pseudo-first-order and

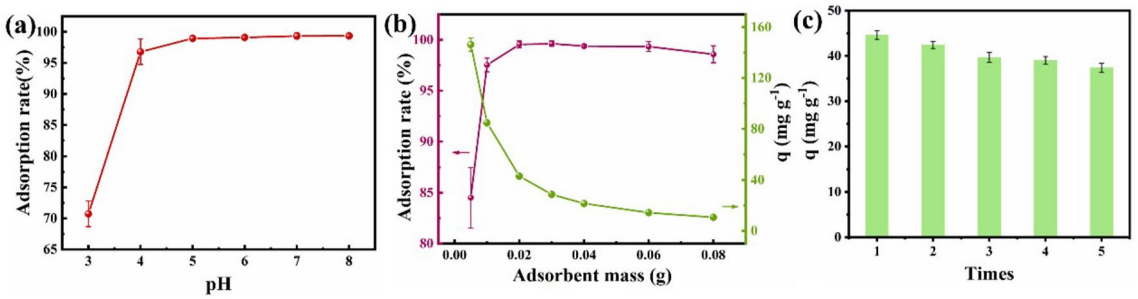

Fig. 3 (Color online) **a** Effect of solution pH on the uranium adsorption rate. **b** Effect of adsorbent mass on the uranium adsorption rate. **c** Cyclic adsorption capacity for 5 times

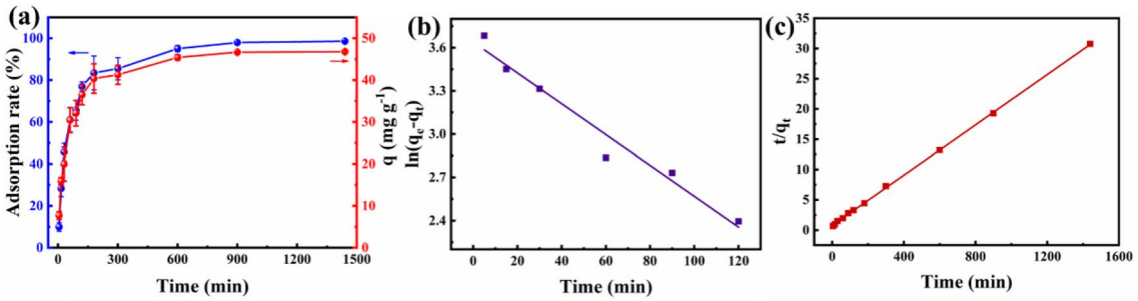

Fig. 4 (Color online) **a** Adsorption kinetics curve. **b** Pseudo-first-order kinetics model. **c** Pseudo-second-order kinetics model

Table 1 Fitting parameters of adsorption kinetics

Kinetics models	Pseudo-first-order			Pseudo-second-order		
	q_e (mg g^{-1})	K_1 (g mg^{-1} min^{-1})	R^2	q_e (mg g^{-1})	K_2 (g mg^{-1} min^{-1})	R^2
Parameters	38.034	0.011	0.957	48.309	5.621×10^{-4}	0.999

pseudo-second-order kinetics models were 0.957 and 0.999, respectively. The theoretical equilibrium adsorption capacity (38.034 mg · g^{-1}) fitted by the pseudo-first-order kinetics model was much smaller than the experimental adsorption capacity (48.311 mg · g^{-1}). In contrast, the pseudo-second-order kinetics model had relatively good fitting results to the kinetics data, and the theoretical equilibrium adsorption capacity (48.309 mg · g^{-1}) was very close to the actual adsorption capacity. It suggests that the adsorption process of CS-BT aerogel is more consistent with the pseudo-second-order kinetics model, thus a chemical adsorption reaction [41].

3.4 Adsorption isotherms

The adsorption isotherms of U(VI) on CS-BT aerogel are shown in Fig. 5a. With the increasing concentration of U(VI), the adsorption capacity of CS-BT aerogel rapidly improved and then gradually slowed down. At the low concentration of U(VI), the adsorbent had relatively abundant active adsorption sites, which allowed rapid and efficient adsorption. As the U(VI) concentration increased, the adsorption sites on CS-BT aerogel became progressively saturated by U(VI), thus reducing the U(VI) concentration difference between adsorbent and solution. The increment of adsorption capacity of CS-BT aerogel gradually slowed down until adsorption equilibrium was achieved. With increasing temperature, the adsorption capacity increased, with 390.11 mg · g^{-1} at 328.15 K. It indicates that high temperature is conducive to the adsorption of CS-BT aerogel toward uranyl ions. The adsorption isotherms data were further nonlinearly fitted by using Langmuir and Freundlich isothermal models. They are based on monolayer adsorption on a homogeneous surface and multilayer adsorption on a heterogeneous surface, respectively [42, 43]. The fitting results are shown in Fig. 5b-c and Table 2. R^2 of Freundlich model was higher than that of Langmuir model, with 0.991 and 0.988 at 328.15 K, respectively. It suggests that the isotherms are well fitted by the Freundlich model, and the adsorption process of U(VI) occurs a multilayer adsorption-dominated mechanism on the heterogeneous surface of CS-BT aerogel [44, 45].

3.5 Adsorption thermodynamics

The equilibrium adsorption capacity of CS-BT aerogel toward U(VI) at different temperatures is shown in Fig. 6a. As the temperature increased, the equilibrium adsorption capacity exhibited a significant upward trend, indicating that the elevated temperature facilitated the adsorption of U(VI) by the CS-BT aerogel. Figure 6b shows the linear fitting curve of $\ln K_0$ versus $1/T$. According to this curve, the thermodynamic data can be obtained, as shown in Table 3. The Gibbs free energies are negative at the four experimental temperatures, indicating U(VI)adsorption on the CS-BT aerogel spontaneously occurs and is thermodynamically feasible. The chelation between -OH, -NH_2, and C=O groups on CS-BT aerogel and U(VI) served as one of the driving forces to promote the spontaneous occurrence of the adsorption process. The negative enthalpy change during the adsorption process indicated that the adsorption of U(VI) by the CS-BT aerogel was an exothermic reaction.

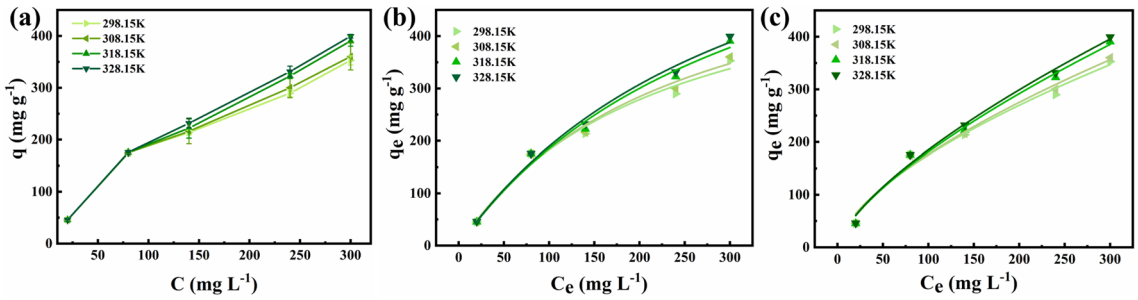

Fig. 5 (Color online) **a** Adsorption kinetics curve. **b** Pseudo-first-order kinetics model. **c** Pseudo-second-order kinetics model

Table 2 Fitting parameters of adsorption isotherms

Isothermal model	Temperature (K)	Langmuir			Freundlich		
		q_m (mg g^{-1})	K_L (L mg^{-1})	R^2	K_F (L $mg^{-1})^{1/n}$	n	R^2
Parameters	298.15	586.27	0.004	0.974	10024.0	1.609	0.974
	308.15	627.67	0.004	0.980	9441.8	1.571	0.981
	318.15	780.00	0.003	0.983	7711.8	1.458	0.986
	328.15	814.42	0.003	0.988	7727.8	1.449	0.991

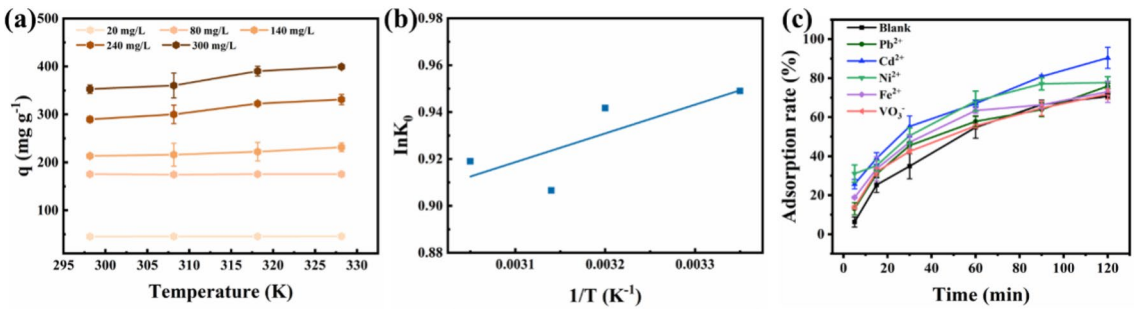

Fig. 6 (Color online) **a** Effect of temperature on the adsorption of U(VI) on CS-BT aerogel. **b** Fitting diagram of $\ln K_0$ versus *1/T* for the adsorption of U(VI) by CS-BT aerogel. **c** The adsorption rate of U(VI) with or without coexisting ions

Consequently, increasing the temperature did not significantly enhance the adsorption efficiency. The entropy change is positive, demonstrating that the adsorption of CS-BT aerogel toward U(VI) is a disordered increasing process on the solid–liquid surface [46].

3.6 Effect of coexisting ions

In practical applications, a variety of coexisting ions are inevitably present in uranium-containing aqueous solutions, and they can also compete with the U(VI) for adsorption, thus affecting the removal efficiency of U(VI) [47]. To assess the influence of coexisting ions on the adsorption effect of U(VI), the removal efficiency of U(VI) was investigated within 120 min in the coexistence solution of different ions. As shown in Fig. 6c, Pb^{2+}, Cd^{2+}, Ni^{2+}, Fe^{3+}, and VO_3^- exhibited minimal inhibitory effects on the adsorption of U(VI) by CS-BT aerogel during the adsorption process. Usually, VO_3^- has strong competition for U(VI) adsorption, but here its effect is not significant [45], which may be due to the fact that VO_3^- does not has a high affinity for -OH groups from the CS-BT aerogel. These results indicate that the adsorption of U(VI) by CS-BT aerogel was minimally affected by other coexisting ions. This excellent selectivity endows the CS-BT aerogel with great potential for practical applications in uranium recovery from both wastewater and seawater.

3.7 Adsorption mechanism

The microscopic morphology of CS-BT aerogel adsorbed U(VI) was also characterized by SEM. As shown in Fig. 7a and b, the blocky solid particles could be observed in the pores and walls of CS-BT aerogel, which should be the uranium aggregate. Meanwhile, the peak of uranium element is also shown in the energy spectrum of Fig. 7c. The average elemental percentages of the energy spectra obtained from the three different sites are shown in Table 4, in which the percentage of uranium is as high as 15.36 ± 5.20%. These results indicate that U(VI) has been successfully uploaded into the CS-BT aerogel.

To further characterize the structure change of CS-BT aerogel after adsorbing U(VI), FTIR and XPS were carried out. As shown in Fig. 7d, a new peak could be observed at 898 cm-1 after the adsorption of CS-BT aerogel toward U(VI), which can be assigned to the characteristic peak of U(VI). The peak at 3419 cm^{-1} corresponded to -OH and $-NH_2$ groups, which became wider, and the phenolic -OH group obviously shifted from 1407 cm^{-1} to 1389 cm^{-1}. It suggests that there is a strong interaction between -OH groups and U(VI). Moreover, a new U 4f peak also could be seen from XPS total spectra in Fig. 7e. And the O 1 s XPS high-resolution spectra in Fig. 7f showed that the peaks of C=O and C-O shifted to higher binding energy (from 531.37 to 532.2 eV and 532.76 to 533.05 eV, respectively) [48], which once again confirms the interaction between CS-BT aerogel and U(VI). These results indicate that the adsorption of CS-BT aerogel toward U(VI) is mainly achieved through the chelation between -OH groups and U(VI) [49]. Based on the above analyses, a possible adsorption mechanism is proposed during the adsorption of CS-BT aerogel toward U(VI) and shown in Fig. 8.

4 Conclusion

In this work, we have fabricated a biomass CS-BT aerogel with porous structure by cross-linking chitosan and bayberry tannin using glutaraldehyde. The cross-linked aerogel confers excellent aqueous stability in water, solving the disadvantage that chitosan and bayberry tannin cannot be directly used in uranium extraction from aqueous solutions due to their inherent water solubility. Because there are several -OH groups on CS-BT aerogel that can chelate with U(VI), CS-BT aerogel shows an excellent adsorption performance toward U(VI), with the maximum adsorption capacity of 140 mg · g^{-1} (at 298.15 K, pH=5.0). The kinetic study reveals that its adsorption is a chemical

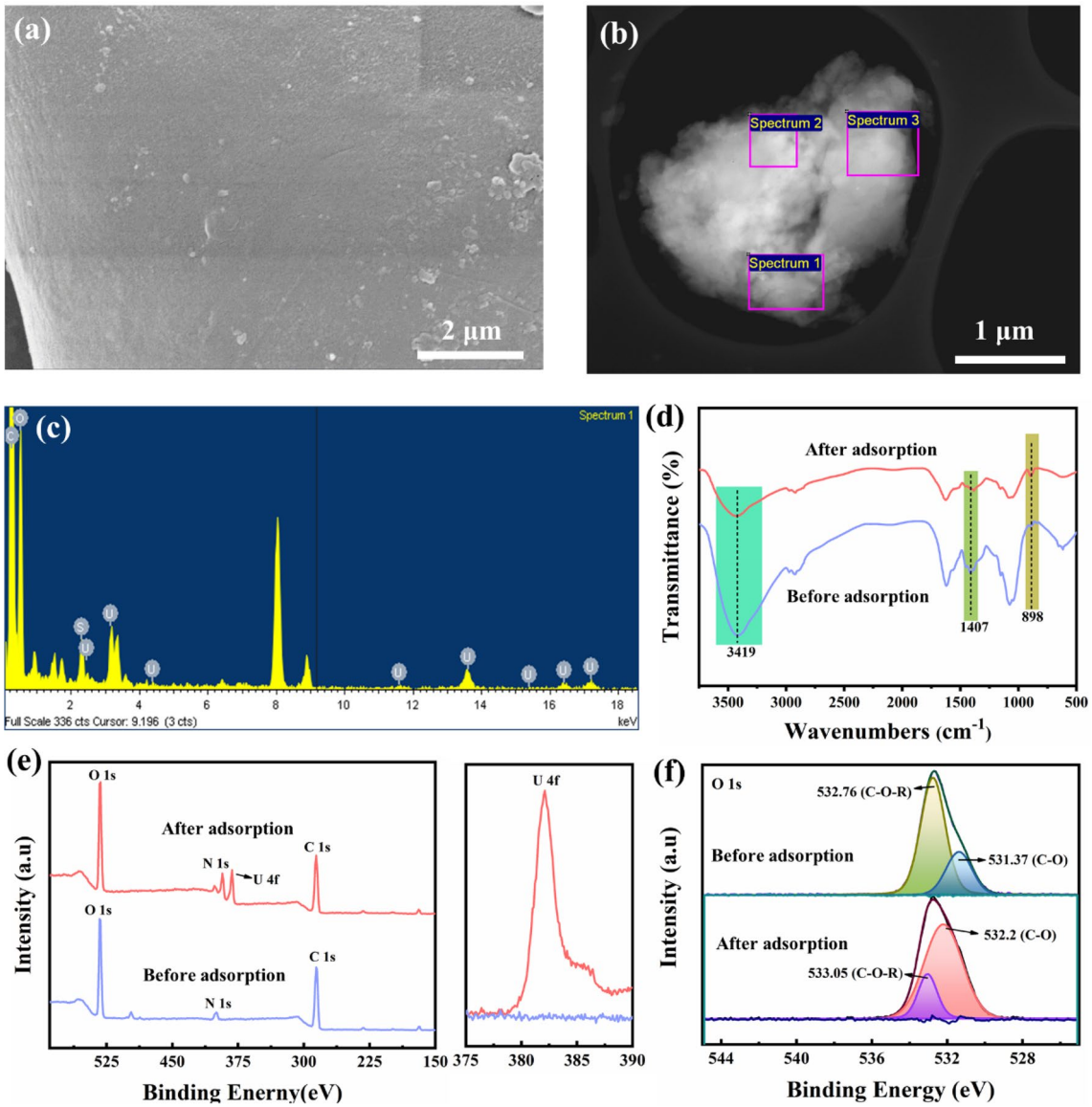

Fig. 7 (Color online) **a**, **b** SEM images of CS-BT aerogel after adsorption. **c** Energy spectrum of CS-BT aerogel after adsorption. **d** FTIR spectra of CS-BT aerogel before and after adsorption. **e** XPS total spectra before and after adsorption of CS-BT composite aerogel. **f** O1s XPS high-resolution spectra

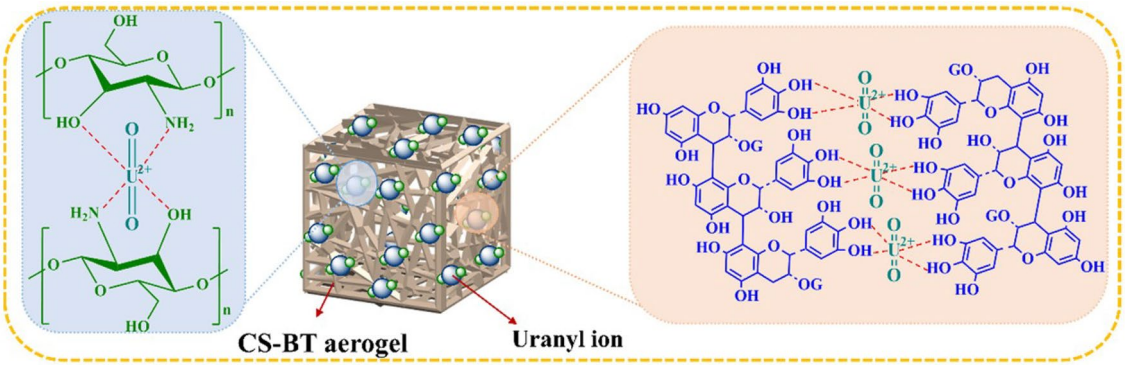

Fig. 8 (Color online) Possible adsorption mechanism of CS-BT aerogel toward U(VI)

Table 3 Thermodynamic parameters of CS-BT composite aerogel

T (K)	ΔH^0 (K ·J · mol^{-1})	ΔS^0 (J mol^{-1} K^{-1})	ΔG^0 (K· J · mol^{-1})
298.15	−1.109	0.004	−2.352
308.15	−1.109	0.004	−2.412
318.15	−1.109	0.004	−2.398
328.15	−1.109	0.004	−2.507

Table 4 Contents of different elements after adsorption

Element	C	O	S	U
Proportion (%)	66.50 ± 2.69	14.89 ± 3.87	3.25 ± 0.94	15.36 ± 5.20

adsorption process dominated by multilayer adsorption. And the thermodynamic study shows that the adsorption process is spontaneous and exothermic. These results demonstrate that the CS-BT aerogel is a promising material for extracting uranium from natural seawater and nuclear industry wastewater. Unlike traditional adsorbent materials, this CS-BT aerogel is made from almost exclusively biomass, reducing carbon emissions during the preparation, and contributing to the sustainability of the nuclear industry.

Author Contributions All authors contributed to the study conception and design. Material preparation, data collection, and analysis were performed by Gui-Qiang He, Jin-Fan Ou, Ai-Xia Lu, and Yan-Xia Wei. The first draft of the manuscript was written by Gui-Qiang He, and all authors commented on previous versions of the manuscript. All authors read and approved the final manuscript.

Data Availability The data that support the findings of this study are openly available in Science Data Bank at https://cstr.cn/31253.11.sciencedb.28427 and https://doi.org/10.57760/sciencedb.28427.

Declarations

Conflict of interest The authors declare that they have no conflict of interest.

References

1. S. Shi, B. Li, Y. Qian et al., A simple and universal strategy to construct robust and anti-biofouling amidoxime aerogels for enhanced uranium extraction from seawater. Chem. Eng. J. **397**, 125337 (2020). https://doi.org/10.1016/j.cej.2020.125337
2. P. Liu, M. An, T. He et al., Recent advances in antibiofouling materials for seawater-uranium extraction: A review. Materials. **16**, 6451 (2023). https://doi.org/10.3390/ma16196451
3. F. Wu, N. Pu, G. Ye et al., Performance and mechanism of uranium adsorption from seawater to poly(dopamine)-inspired sorbents. Environ. Sci. Technol. **51**, 4606 (2017). https://doi.org/10.1021/acs.est.7b00470
4. L. Rani, A.L. Srivastav, J. Kaushal et al., Significance of MOF adsorbents in uranium remediation from water. Environ. Res. **236**, 116795 (2023). https://doi.org/10.1016/j.envres.2023.116795
5. Y. Qian, Y. Yuan, H. Wang et al., Highly efficient uranium adsorption by salicylaldoxime/polydopamine graphene oxide nanocomposites. J. Mater. Chem. A. **6**, 24676 (2018). https://doi.org/10.1039/c8ta09486a
6. D. Zhang, L. Fang, L. Liu et al., Uranium extraction from seawater by novel materials: A review. Sep. Purif. Technol. **320**, 124204 (2023). https://doi.org/10.1016/j.seppur.2023.124204
7. J. Xu, J. Leddy, C. Korzeniewski, Cyclic voltammetry as a probe of selective ion transport within layered, electrode-supported ion-exchange membrane materials. J. Electrochem. Soc. **169**, 026520 (2022). https://doi.org/10.1149/1945-7111/ac51fd
8. P. Suresh, C.E. Duval, Poly(acid)-functionalized membranes to sequester uranium from seawater. Ind. Eng. Chem. Res. **59**, 12212 (2020). https://doi.org/10.1021/acs.iecr.0c01090
9. J. Yu, H. Zhang, Q. Liu et al., A high-flux antibacterial poly(amidoxime)-polyacrylonitrile blend membrane for highly efficient uranium extraction from seawater. J. Hazard. Mater. **440**, 129735 (2022). https://doi.org/10.1016/j.jhazmat.2022.129735
10. F. Zhang, H. Zhang, R. Chen et al., Mussel-inspired antifouling magnetic activated carbon for uranium recovery from simulated seawater. J. Colloid Interf. Sci. **534**, 172 (2019). https://doi.org/10.1016/j.jcis.2018.09.023
11. A.S. Ivanov, B.F. Parker, Z. Zhang et al., Siderophore-inspired chelator hijacks uranium from aqueous medium. Nat. Commun. **10**, 819 (2019). https://doi.org/10.1038/s41467-019-08758-1
12. V. Gomase, P. Doondani, D. Saravanan et al., A novel Chitosan-Barbituric acid hydrogel supersorbent for sequestration of chromium and cyanide ions: Equilibrium studies and optimization through RSM. Sep. Purif. Technol. **330**, 125475 (2024). https://doi.org/10.1016/j.seppur.2023.12547
13. S. Pandey, S. Kim, Y.S. Kim et al., Fabrication of next-generation multifunctional LBG-s-AgNPs@ g-C3N4 NS hybrid nanostructures for environmental applications. Environ. Res. **240**, 117540 (2024). https://doi.org/10.1016/j.envres.2023.117540
14. S. Pandey, S.B. Mishra, Organic-inorganic hybrid of chitosan/organoclay bionanocomposites for hexavalent chromium uptake. J. Colloid Interf. Sci. **361**, 509 (2011). https://doi.org/10.1016/j.jcis.2011.05.031
15. V.K. Saruchi, D. Bhatt et al., Gum katira-silver nanoparticle-based bionanocomposite for the removal of methyl red dye. Front. Chem. **10**, 959104 (2023). https://doi.org/10.3389/fchem.2022.959104
16. Z. Li, R. Zhu, P. Zhang et al., Functionalized polyarylether-based COFs for rapid and selective extraction of uranium from aqueous solution. Chem. Eng. J. **434**, 134623 (2022). https://doi.org/10.1016/j.cej.2022.134623
17. K. Sang, Y. Wang, Y. Wang et al., Hypercrosslinked phenylalaninol for efficient uranium adsorption from water. Sep. Purif. Technol. **305**, 122292 (2023). https://doi.org/10.1016/j.seppur.2022.122292
18. H. Mittal, A.M. Alfantazi, S.M. Alhassan, Recent developments in the adsorption of uranium ions from wastewater/seawater using carbon-based adsorbents. J. Environ. Chem. Eng. **12**, 111705 (2024). https://doi.org/10.1016/j.jece.2023.111705
19. J. Lei, H. Liu, L. Zhou et al., Progress and perspective in enrichment and separation of radionuclide uranium by biomass functional materials. Chem. Eng. J. **471**, 144586 (2023). https://doi.org/10.1016/j.cej.2023.144586
20. Y. Wang, Y. Li, Y. Zhang et al., Nanocellulose aerogel for highly efficient adsorption of uranium (VI) from aqueous solution. Carbohyd. Polym. **267**, 118233 (2021). https://doi.org/10.1016/j.carbpol.2021.118233

21. Y. Pu, T. Qiang, L. Ren, Waste feather fiber based high extraction capacity bio-adsorbent for sustainable uranium extraction from seawater. Int. J. Biol. Macromol. **206**, 699 (2022). https://doi.org/10.1016/j.ijbiomac.2022.03.019
22. M. Cao, Q. Peng, Y. Wang et al., High-efficiency uranium extraction from seawater by low-cost natural protein hydrogel. Int. J. Biol. Macromol. **242**, 124792 (2023). https://doi.org/10.1016/j.ijbiomac.2023.124792
23. J. Zhu, Y. Luo, J. Wang et al., Highly efficient uranium extraction by aminated lignin-based thermo-responsive hydrogels. J. Mol. Liq. **368**, 120744 (2022). https://doi.org/10.1016/j.molliq.2022.120744
24. Y. Wang, Y. Zhang, Q. Li et al., Amidoximated cellulose fiber membrane for uranium extraction from simulated seawater. Carbohyd. Polym. **245**, 116627 (2020). https://doi.org/10.1016/j.carbpol.2020.116627
25. X. Ye, R. Chi, Z. Wu et al., A biomass fiber adsorbent grafted with phosphate/amidoxime for efficient extraction of uranium from seawater by synergistic effect. J. Environ. Manage. **337**, 117658 (2023). https://doi.org/10.1016/j.jenvman.2023.117658
26. G. Zhang, D. Shao, H. Yu et al., MXene Nanosheet-Enhanced Chitin Aerogel Spheres for Bilirubin Adsorption. ACS Appl. Nano Mater. **5**, 17293 (2022). https://doi.org/10.1021/acsanm.2c04461
27. R. Wang, M. Li, T. Liu et al., Encapsulating carbon-coated nano zero-valent iron particles with biomass-derived carbon aerogel for efficient uranium extraction from uranium-containing wastewater. J. Clean. Prod. **364**, 132654 (2022). https://doi.org/10.1016/j.colsurfa.2021.127527
28. Y. Pu, T. Qiang, G. Li et al., Efficient adsorption of low-concentration uranium from aqueous solutions by biomass composite aerogel. Ecotoxi. Environ. Safe. **259**, 115053 (2023). https://doi.org/10.1016/j.ecoenv.2023.115053
29. Z. Du, Y. Ni, H. Peng et al., Adsorption of U(VI) by chitosan crosslinked PAO aerogel. J. Radioanal. Nucl. Ch. **333**, 71 (2023). https://doi.org/10.1007/s10967-023-09261-0
30. X. Jiang, H. Wang, E. Hu et al., Efficient adsorption of uranium from aqueous solutions by microalgae based aerogel. Micropor. Mesopor. Mat. **305**, 110383 (2020). https://doi.org/10.1016/j.micromeso.2020.110383
31. X. Qiu, Y. Shen, R. Yang et al., Adsorption of RE3+ from aqueous solutions by bayberry tannin immobilized on chitosan. Environ. Technol. **40**, 202 (2017). https://doi.org/10.1080/09593330.2017.1384072
32. T. Zhang, Y. Wang, Y. Kuang et al., Adsorptive removal of Cr 3+ from aqueous solutions using chitosan microfibers immobilized with plant polyphenols as biosorbents with high capacity and selectivity. Appl. Surf. Sci. **404**, 418 (2017). https://doi.org/10.1016/j.apsusc.2017.02.018
33. S. Fan, J. Chen, C. Fan et al., Fabrication of a CO2-responsive chitosan aerogel as an effective adsorbent for the adsorption and desorption of heavy metal ions. J Hazard. Mater. **416**, 126225 (2021). https://doi.org/10.1016/j.colsurfa.2023.132754
34. L. Yang, C. Huang, X. Luo et al., Chitosan-based aerogel with anti-swelling for U(VI) adsorption from aqueous solution. Colloid. Surface. A. **630**, 127527 (2021). https://doi.org/10.1016/j.colsurfa.2021.127527
35. S. Li, Y. Li, Z. Fu et al., A 'top modification' strategy for enhancing the ability of a chitosan aerogel to efficiently capture heavy metal ions. J. Colloid Interf. Sci. **594**, 141 (2021). https://doi.org/10.1016/j.jcis.2021.03.029
36. W.S.W. Ngah, S. Fatinathan, Adsorption of Cu(II) ions in aqueous solution using chitosan beads, chitosan-GLA beads and chitosan-alginate beads. Chem. Eng. J. **143**, 62 (2008). https://doi.org/10.1016/j.cej.2007.12.006
37. Y.-W. Chen, J.-L. Wang, Removal of cesium from radioactive wastewater using magnetic chitosan beads cross-linked with glutaraldehyde. Nucl. Sci. Tech. **27**, 43 (2016). https://doi.org/10.1007/s41365-016-0033-6
38. F. Doustdar, A. Olad, M. Ghorbani, Effect of glutaraldehyde and calcium chloride as different crosslinking agents on the characteristics of chitosan/cellulose nanocrystals scaffold. Int. J. Biol. Macromol. **208**, 912 (2022). https://doi.org/10.1016/j.ijbiomac.2022.03.193
39. Z. Zhang, L. Wang, H. Yu et al., Highly Transparent, Self-Healable, and Adhesive Organogels for Bio-Inspired Intelligent Ionic Skins. ACS Appl. Mater. Interfaces. **12**, 15657 (2020). https://doi.org/10.1021/acsami.9b22707
40. Q. Xin, Q. Wang, K. Luo et al., Mechanism for the selective adsorption of uranium from seawater using carboxymethyl-enhanced polysaccharide-based amidoxime adsorbent. Carbohyd. Polym. **324**, 121576 (2024). https://doi.org/10.1016/j.carbpol.2023.121576
41. X. Liu, K. Jing, S. Peng et al., Facile preparation of graphene oxide-based composite aerogel to efficiently adsorb methylene blue. Colloid. Surface. A. **681**, 132754 (2024). https://doi.org/10.1016/j.colsurfa.2023.132754
42. Y.-R. He, S.-C. Li, X.-L. Li et al., Graphene (rGO) hydrogel: A promising material for facile removal of uranium from aqueous solution. Chem. Eng. J. **338**, 333 (2018). https://doi.org/10.1016/j.cej.2018.01.037
43. Z. Huang, Z. Li, L. Zheng et al., Interaction mechanism of uranium(VI) with three-dimensional graphene oxide-chitosan composite: Insights from batch experiments, IR, XPS, and EXAFS spectroscopy. Chem. Eng. J. **328**, 1066 (2017). https://doi.org/10.1016/j.cej.2017.07.067
44. F. Yu, F. Song, R. Wang et al., Sulfonated perylene-based conjugated microporous polymer as a high-performance adsorbent for photo-enhanced uranium extraction from seawater. Polym. Chem. **12**, 867 (2021). https://doi.org/10.1039/d0py01656j
45. Q. Xin, Q. Wang, J.G. A, et al., Enhanced performance in uranium extraction by the synergistic effect of functional groups on chitosan-based adsorbent. Carbohyd. Polym. **300**, 120270 (2023). https://doi.org/10.1016/j.carbpol.2022.120270
46. T. Liu, J. Ma, X. Li et al., Efficient removal of U(VI) by an environmental-friendly amidoxime matrix microspheres: Batch experiments and mechanism investigation. J. Environ. Chem. Eng. **11**, 110151 (2023). https://doi.org/10.1016/j.carbpol.2023.121576 10.1016/j.jece.2023.110151
47. R. Yu, Y. Lu, X. Zhang et al., Amidoxime-modified ultrathin polyethylene fibrous membrane for uranium extraction from seawater. Desalination **539**, 115965 (2022). https://doi.org/10.1016/j.desal.2022.115965
48. N. Li, J. Wu, R. Su et al., Bioinspired green tea waste/graphene aerogel for solar-enhanced uranium extraction from seawater. Desalination **545**, 116153 (2023). https://doi.org/10.1016/j.desal.2022.116153
49. M.A. Rahim, G. Lin, P.P. Tomanin et al., Self-Assembly of a Metal-Phenolic Sorbent for Broad-Spectrum Metal Sequestration. ACS Appl. Mater. Interfaces. **12**, 3746 (2020). https://doi.org/10.1021/acsami.9b19097